Effect of the Green Synthesized rGO and Mg/rGO Nanocomposites Using High Molecular Weight Polyphenols of *Rosa Canina* Fruit and Investigation of Their Effects on Phytochemical Assay and Toxicity in Organ Culture of *Mentha Longifolia*

Saeed Jafarirad (jafarirad@tabrizu.ac.ir)
University of Tabriz https://orcid.org/0000-0001-6609-8686
Morteza Kosari-Nasab
University of Tabriz
Monireh Aminpour
University of Tabriz
Zahra Rezaei
University of Tabriz

Research Article

Keywords: High molecular weight polyphenols, Mg/rGO nanocomposites, Mentha longifolia, oxygenated terpenoids

Posted Date: May 27th, 2021

DOI: https://doi.org/10.21203/rs.3.rs-474307/v1

Abstract

Reduced graphene oxide (rGO) and Mg/rGO nanocomposites (NCs) were prepared by an eco-friendly technique using high molecular weight polyphenols of *Rosa canina* fruit. Physicochemical properties and cytotoxicity to *Mentha longifolia in vitro* cultures of these nanomaterials were examined by using XRD, FESEM, EDX, FTIR, DLS/Zeta potential, UV–Visible and GC-MS techniques. The characterization techniques confirmed the synthesis of rGO and Mg/rGO NCs with particle sizes less than 20 nm (based on FESEM). In accordance to the biological measurements, rGO showed *in vitro* cytotoxicity to *M. longifolia* shoot cultures. Mg/rGO NCs showed no significant difference in the growth parameters except for a decrease in the soot number at the concentrations of 50 and 150 mg/L and a decrease in the length of the tallest root at the concentrations of 100 and 150 mg/L, however, efficiently improved the photosynthetic pigment contents. The phytochemical assay depicted that the total content of volatile compounds was increased in the treated cultures with 25, 50, and 100 mg/L of rGO and Mg/rGO NCs in comparison to the control. Generally, the more oxygenated and hydrocarbon sesquiterpenes was observed in the cultures treated with 25 and 100 mg/L of rGO and 25 and 50 mg/L of Mg/rGO NCs.

Introduction

Because of useful physicochemical properties, low cost, and availability for mass production, graphene-based nanomaterials (NMs) have been found to be promising agents for various applications in electronics, energy storage, catalysis, drug delivery, cancer imaging, and photothermal therapy (Fan et al., 2015; Jafarirad et al., 2018; Li et al., 2013; Wu et al., 2015). It has been revealed that these NMs also show a high antimicrobial ability (Zhu et al., 2017). Besides, they have been considered as basic units for fabricating functional nanocomposites (NCs), incorporated with polymers, metals, metal oxides, and organic crystals for a range of utilization (Huang et al., 2012). Among them, reduced graphene oxide (rGO), as an important derivative of graphene family, has been suggested to be a favorite candidate for the immobilization of metal nanoparticles (NPs) (Julkapli and Bagheri, 2015; Tan et al., 2013). Recently, magnesium (Mg)-based nanomaterials have attracted researchers attention because of the special characteristics such as low weight, harmlessness, high specific stiffness, noncorrosive, thermally stable, and electromagnetic shielding properties (Alavi and Morsali, 2010). It has been proposed that Mg-based/rGO NCs are promising NMs for energy storage devices and sensitive biosensors (Asif et al., 2017; Bhargava and Khan, 2017).

Various chemical and thermal reduction methods has been reported for the successfully synthesis of rGO and their NCs with metal nanoparticles (Chen et al., 2012). However, encounter problems such as high cost and use of toxic reducing agents (for instance hydrazine, di-methylhydrazine, hydroquinone, sodium borohydride etc.) have steered researchers to focus on the alternative synthesize methods, particularly for NMs with bio-related applications (De Silva et al., 2017). Accordingly, green synthetic approaches using some plant extracts such as *Euphorbia wallichii* (Atarod et al., 2015), grape (Upadhyay et al., 2015) and *Hibiscus sabdariffa* (Nazari et al., 2018) have been applied for the reduction of GO and GO-based NCs in order to overcome the above mentioned problems. *Rosa canina* L. (Rosaseae family) is a known

medicinal plant with various traditional uses. It has been reported that the fruit extracts of this plant exhibit anti-inflammatory, antioxidant, and antiproliferative activities (Lattanzio et al., 2011; Tumbas et al., 2012). According to the phytochemical studies, the aqueous extract of *R. canina* fruit is rich of high molecular weight polyphenols, lignins and tannins (Roman et al., 2013). These bioactive compounds can act as reducing and stabilizing agents for NMs preparation (Nazari et al., 2020; Veisi et al., 2016).

Latest investigations have revealed that NMs have significant effects on plant growth, development, and physiology. Several phytotoxicity studies demonstrated that GO could be transported and accumulated in plant tissues and consequently affected their physiological responses (Anjum et al., 2013; Zhao et al., 2015). Nonetheless, their effect on plant metabolism is still unknown. Metabolomics analyses can be used to reveal the mechanisms of toxicity of NMs in plants. Indeed, metabolic alterations reflect biological processes in a direct way (Hu et al., 2014). So far, some metabolomics-based studies have been provided valuable information about the changes in metabolites and biochemical pathways in response to various environmental stressors (Shulaev et al., 2008; Wu et al., 2017). Beside toxic effects, NMs-mediated changes in the metabolism could also be beneficial. It has been suggested that some NMs can be used as elicitors to enhance the production of desired secondary metabolites such as artemisinin and diosgenin (Marslin et al., 2017). Also, nano-biofertilizers intended to improve crop production and plant nutrition (Subramanian et al., 2015). Therefore, investigations on the changes in primary and secondary metabolism in response to NMs stress are crucial to tackle the adverse effects or take advantage of the positive impacts such as manipulating the production of valuable compounds.

Mentha longifolia (Lamiaceae) is an aromatic medicinal plant traditionally used as medicine for the treatment of lots of diseases and disorders. Several pharmacological properties of *M. longifolia* including antibacterial, anti-inflammatory, and antioxidant activities can be associated with the bioactive metabolites such as flavonoids, phenolic acids, terpenoids, and essential oils (Asghari et al., 2018). Monoterpenes such as pulegone, menthone, isomenthone, menthol, 1,8-cineole, borneol, and piperitenone have been reported as the main volatile compounds of this plant (Mikaili et al., 2013). In this work, the main aim was to study the metabolic response of *M. longifolia* to rGO and Mg/rGO NCs treatments. Accordingly, the rGO and Mg/rGO were synthesized by using aquatic fruit extract of *R. canina* as a reducing and stabilizing agents. As-prepared rGO and Mg/rGO NCs were characterized by various techniques such as Uv-Vis spectroscopy, XRD, FESEM, EDX, FT-IR, and DLS. Subsequently, the growth characteristic and photosynthetic pigments contents of *M. longifolia in vitro* cultures were measured under the synthesized NMs stress. Finally, the changes in metabolite profiles were analyzed using GC-MS-based metabolomics.

Materials And Methods

Preparation of rGO

A modified Hummer synthesize method was applied for the preparation of GO (Wang et al., 2009). Initially, 5 g of graphite powder and 2.5 g of $NaNO_3$ were stirred in 115 mL of concentrated H_2SO_4 at the

temperature of 0 °C. Subsequently, 15 g of $KMnO_4$ was slowly added to the mixture under constant stirring at 35 °C. The mixture's temperature was kept at 35 °C for 30 min. Then, 230 mL of deionized water was added and followed by the addition of 700 mL of hot deionized water and 12.5 mL of 30% H_2O_2 solution after 15 min. After washing with dilute HCl solution and deionized water, the obtained sediment was dried at 50 °C for 3 h.

For the preparation of rGO, 50 mg of GO was dispersed in 90 mL of deionized water using an ultrasonic bath sonicator for approximately 30 min. The obtained suspension was mixed with 15 mL of *R. canina* fruit extract prepared according to the method described previously (Nazari et al., 2020) and was subjected to reflux. As-synthesized rGO was dried after washing with deionized water.

Preparation of Mg/rGO NCs using both heating (H) and microwave (M) irradiation methods

For the green synthesis of Mg/rGO NCs, 0.053 g of the synthesized GO was mixed in 4 mL of deionized water and placed in an ultrasonic bath for 2 h. Then, 0.045 g of $Mg(NO_3)_2.6H_2O_2$ was mixed in 6 mL of deionized water and gradually added to the stable GO dispersion. The obtained mixture was put in an ultrasonic bath for 3 h and refluxed for 20 h at 45 °C. Subsequently, 15 mL of *R. canina* extract was added to the reaction mixture and refluxed for 24 h at 90 °C. Finally, the obtained product was collected and washed several times with deionized water and dried at 50 °C for 3 h.

In an alternative method, Mg/rGO NCs was also prepared using M method. In this direct, the above-mentioned method (H) was used except that the mixture was placed under microwave irradiation at 900 W during 7 minutes instead of reflux for 24 h at 90 °C . Finally, the obtained product was collected and washed several times with deionized water and dried at 50 °C for 3 h.

Characterization of rGO and Mg/rGO NCs

The synthesized rGO and Mg/rGO NCs were characterized using UV-Vis spectrophotometer (Unico, S2100, USA), field emission scanning electron microscope equipped with energy dispersive X-ray analysis (Hitachi, 4200, Japan), X-ray powder diffraction (PANalytical X'Pert PRO-Germany), dynamic light scattering (Nanotrac Wave), and fourier transform infrared (Tensor 27, Bruker, Germany) techniques.

In vitro cultures and treatments

Surface sterilization of *M. longifolia* seeds was down using 70% ethanol (3 min) and 20% sodium hypochlorite (15 min) followed by repeated washes with sterile distilled water. Then, the seeds were germinated on solidified Murashige and Skoog (MS) medium (0.8% agar, pH 5.6-5.8) at 25 ± 1 °C under continuous light for 21 days. Subsequently, shoot cultures were initiated by transferring stem explants with 2-3 nodes to solid MS medium containing 0.8% agar, 3% sucrose, and different concentrations of rGO and Mg/rGO NCs (prepared by CH method) (0, 25, 50, 100, and 150 mg/L) with pH 5.6-5.8 and kept at under 24 h light photoperiod at 24 ± 1 ˚C for 28 days.

Measurement of growth characteristic

In order to investigate the effect of rGO and Mg/rGO NCs on growth characteristic of *M. longifolia* shoot cultures, the final fresh weight (FW), dry weight (DW, dried at 35 ^{o}C for 24 h), the number of nodes, leaves, shoots, and roots, the length of the smallest shoot and root were measured.

Quantification of photosynthetic pigments

Harvested shoots were homogenized in dimethyl sulfoxide solvent and centrifuged at 5900 J for 15 min. The absorbance of the supernatant was determined at 480, 649, and 665 nm. Chlorophylls and carotenoids contents were calculated according to the equations described by (Wellburn, 1994):

$C_a = 12.19A_{665} - 3.45A_{649}$

$C_b = 21.99A_{649} - 5.32A_{665}$

$C_{x+c} = (1000A_{480} - 1.14C_a - 70.16C_b)/220$

GC-Mass analysis

Extraction of volatile compounds was carried out using the method reported by (Barazani et al., 1999). Briefly, 200 mg of plantlets of treated (except for the cultures exposed to 150 mg/L of rGO and 150 mg/L Mg/rGO NCs) and untreated shoot cultures were extracted by n-hexane solvent (7 mL) and subjected to GC-MS analysis (Agilent MS 5973 N) with a HP 5MS column (30 m, 0.25 mm, 0.25 µm film thickness). The injection volume and injector temperatures were 1 µl and 150 °C, respectively. The temperature program was used as follows: 70 °C for 3 min, 10 °C/min to 120 °C, 120 °C for 2 min, 10 °C/min to 150 °C, 150 °C for 2 min, 7 °C/min to 240 °C, 240 °C for 5 min. The carrier gas was helium with a flow rate of 1 mL/min. The standard of n-alkanes containing n and n+1 carbons (Sigma) was used to calculate the retention indices (RI) using a generalized equation (Van den Dool and Kratz, 1963). Further identification was made by the comparison of the mass spectra of compounds with the NIST standard reference database.

Statistical Analysis

All the experiments consisted of three replicates with 8 explants per treatment. Statistical significant differences between groups were determined using analysis of variance (ANOVA) test with the statistical software SPSS19. Statistical significance was considered at p values less than 0.05.

Results And Discussion

Nanomaterial characteristics

In the present study, rGO and Mg/rGO NCs were synthesized using *R. canina* fruit extract. In order to determine the properties of the desired NMs, first of all, the reduction of GO to rGO and synthesis of Mg/rGO NCs were monitored using UV-Vis spectroscopy. The UV-Vis spectrum of the synthesized rGO

showed absorption peaks in the range of 270 to 300 nm (Fig. 1A). The peak at λ_{max} 281 nm confirmed the formation of rGO. Furthermore, the absorption at wavelength 254-285 nm was obtained for Mg/rGO NCs indicating the formation of Mg NPs (Fig. 1B, C). In addition, XRD analysis of rGO (Fig. 1D) showed main diffraction peaks at 2θ of 26.62º and 43º which can be attributed to (002) and (001) planes of rGO (Thakur and Karak, 2012). The peaks that appear above the diffraction angle 30º can be indexed to the reflection placed on 2θ of 37.08º, 39.24º, 43.83º, 45.31º and 62.84º of the MgO structure in the Mg/rGO NCs (Fig. 1E, F) (Kanagesan et al., 2013; ullah Rather, 2014). Small peaks of MgO in the as-synthesized NCs are owing to the easy oxidation of magnesium. The average size of rGO calculated by Debye–Scherrer formula were 15.73 nm (Table 1) (Behzad et al., 2020). In addition, the average size of Mg nanoparticles on the surface of rGO in Mg/rGO NCs, for both H and M methods, was 16.86 and 26.88 nm, respectively (Fig. 1E, F).

On the other hand, the particle size and morphology of rGO, Mg/rGO NCs were investigated using FESEM (Fig. 2 A-C). Figures 2B and 2C confirms the presence of spherical Mg nanoparticles in the matrix of Mg/rGO NCs, for both H and M methods, with the average particle size of 14-18 and 11-13 nm, respectively. The elemental composition of rGO and Mg/rGO NCs are presented in figure 2D-F. The existence of Mg (0.48%), carbon (49.65%), and oxygen (49.87%) proves the formation of Mg/rGO NCs (Fig. 2E).

The hydrodynamic diameter of the rGO and the NCs was measured in 25 ^{o}C (Fig, 3 A-C). The PDI of rGO and Mg/rGO NCs, for both H and M methods, were determined as 0.377, 0.444 and 1.132, respectively (Table 1). The average particle size of rGO and Mg/rGO NCs, for both H and M method, determined as 62.19, 171.9, and 289.3 nm, respectively (Table 1). Commonly, the particle size measured by the DLS technique is greater than the size obtained from the FESEM and XRD results. This is due to the fact that DLS technique measures the hydrodynamic diameter of particles in solution, while FESEM measures the diameter of dried particles. The zeta potentials of rGO and Mg/rGO NCs, for both H and M methods, were +32.1, −25.5 and −15.8 mV, respectively. Based on Table 1, the data obviously highlight that the Mg/rGO NCs obtained from M method differ from those obtained using H method in respect of colloidal properties. Notably, these data depict that the colloidal properties of the as-synthesized NCs are in direct relation with the thermal sources during synthetic process (Nazari et al., 2020). Therefore, considering the suitable aspects of H method relative to M in respect of size, PDI and zeta potentials of the synthesized NCs, Mg/rGO NCs obtained from H was selected for evaluating their effects on *M. longifolia* cultures.

The FT-IR spectra of *R. canina* fruit extract, rGO and Mg/rGO, for both H and M methods, are seen in figure 3D-G. The figure 3F, 3G clearly shows metal-oxygen absorption bands on 600-800 cm^{-1} for H and M mehtods, respectively (Jafarirad et al., 2019; Kandiban et al., 2015; Rezaei et al., 2019). Moreover, the bands at 1109, 1074 and 1127 cm^{-1} correspond to C-O stretching mode of esters. In rGO and Mg/rGO NCs (Fig. 3D-G) there are bands due to C=C skeletal aromatic ring vibrations (1630 cm^{-1}) (Ebadollahi et al., 2019) and C–OH bending vibrations (1410 cm^{-1}). The peaks at 1733 cm^{-1} indicates C=O of esters (Fig. 3G) (Rezaei et al., 2019). The band at 2813 cm^{-1} and 2931 cm^{-1} can be attributed to C-H stretching.

In FT-IR spectra of all samples (Fig. 3D-G), the typical peak at 3000-3500 cm^{-1} corresponding to the O-H and N-H groups (Rezaei et al., 2019). Thus, the presence of fruit polyphenols like A-type proanthocyanidin as capping agents in the matrix of rGO and Mg/rGO NCs was confirmed.

Fig. 4 shows the suggested mechanism for the stabilizing effects of the *R. canina* fruit extract. As previously was pointed out it is rich of several secondary methabolites such as polyphenols and tannins (Roman et al., 2013). According to the suggested mechanism, the hydroxyl groups of A-type proanthocyanidin can chelated with the magnesium cations in medium. In addition, A-type proanthocyanidin caused van der Waals bonding with epoxy and carboxyl groups of graphene oxide surface and reduced them relatively (Behzad et al., 2020; Jafarirad et al., 2018; Jafarirad et al., 2019).

Morphological observations of leaves using SEM

SEM was used to investigate leaf surface morphology of the control plants, treated cultures with 150 mg/L of rGO and Mg/rGO NCs. The leaf of *M. longifolia* in control group showed epidermal cells arranged on a regular basis (Fig. 5A). However, rGO treated plants exhibited irregular and swelling cells with the closed stomata compared to the control (Fig. 5B). The regularly shaped epidermal cells were evident in the leaf of treated cultures with Mg/rGO NCs. Only some of the stomata were identified as closed (Fig. 5C). Similarly, it has been reported that 500 mg/L of CNTs caused the formation of the elongated, irregularly shaped cells and epidermis swelling in red spinach. Some stomata of the leaves exposed to CNTs were closed (Begum et al., 2011). According to the reports, stomata closure is one of the most common plant response to the environmental stresses in order to prevent water losses which leads to decreased CO_2 concentration and formation of the reduced forms of electron acceptors in the photosynthetic electron transport chain. Subsequently, this phenomenon can result in production of free radicals and oxidative damages (Mohammadi et al., 2016).

Growth properties

The impact of rGO NPs and Mg/rGO NCs on the growth parameters of *M. longifolia* is presented in Table 2. The number of nodes and leaves were observed to be less in the treated cultures with rGO, but no significant difference was evident in the treated cultures with Mg/rGO NCs when compared to the control. The experiments showed that all the applied concentrations of rGO along with 50 and 150 mg/L of Mg/rGO NCs caused a decrease in the number of shoots. In case of the number of roots, there was no significant difference in rGO and Mg/rGO NCs treatments, except for a decline in the root number at the concentrations of 100 and 150 mg/L of rGO in comparison to the control. An increase in the smallest shoot length of *M. longifolia* was measured in the cultures treated with 25 mg/L of rGO and 150 mg/L of Mg/rGO NCs. The length of the tallest root showed a decrease in the concentrations of 50-150 mg/L of rGO and 100 and 150 mg/L of Mg/rGO NCs (Table 2, Fig. 5 D-F). In addition, no significant differences were found in the fresh and dry weight of the cultures exposed to both rGO and Mg/rGO NCs.

According to the growth measurements, the potential toxicity of rGO on *M. longifolia* plant was approved. The negative impact of graphene-based materials on the growth of several plants such as cabbage,

tomato, red spinach, and rapeseed has also earlier demonstrated (Begum et al., 2011; Cheng et al., 2016). Mg, as an important nutrient, is the structural component of chlorophyll and many co-enzymes involved in several biological activities; it is necessary for plant growth and development and has a key role in plant defense system in stress conditions. Therefore, it seems that the direct availability of Mg in the culture medium released from Mg/rGO NCs is probably required to improve the plant tolerance to rGO stress. On the other hand, it has been reported that Mg-based NPs exhibit positive effects on the photosynthetic activity and growth in plants (Raliya et al., 2014; Rathore and Tarafdar, 2015). Findings suggest that the nano-biofertilizers not only can supply the desired nutrients for the plant but also help in the facile uptake and transport of available nutrients resulting in enhanced crop growth and yield (Benzon et al., 2015). Therefore, there is need for a deeper and more systematic assessment to investigate the ability of Mg/rGO NCs as Mg nano-fertilizer in plants.

Photosynthetic Pigment Composition

The results in Table 3 suggest that the content of chlorophyll a, b and carotenoids were sensitive to rGO and Mg/rGO NCs exposure in *M. longifolia in vitro* cultures. Spectrophotometric analysis showed that treated cultures with rGO revealed a significant decrease in chlorophyll and carotenoid contents, except for the cultures exposed to 100 mg/L of rGO, which showed no significant difference in the content of photosynthetic pigments when compared with the control. In contrast, Mg/rGO NCs augmented the content of chlorophyll a at the concentrations of 25, 50, and 100 mg/L and chlorophyll b at the concentrations of 25 and 100 mg/L in comparison with the control. Carotenoid contents were also increased in all applied concentrations of Mg/rGO NCs. The highest chlorophyll a and carotenoid concentrations were observed in the cultures treated with 50 mg/L of Mg/rGO NCs compared to other treated cultures and the control. The 25 mg/L Mg/rGO NCs treated cultures showed the highest chlorophyll b concentrations as well.

The decline in the levels of photosynthetic pigments and severe structural damage to the chloroplast under the influence of GO has been already reported in previous reports. It has been suggested that significant reduction of photosynthetic pigments content, particularly chlorophyll a, can be considered as a notable indicator to detect stress induced by NMs. Indeed, the adverse impact of NMs on photosynthesis and chloroplast degradation could be connected to the oxidative stress induced by NMs (Hazeem et al., 2017; Hu et al., 2014). However, considering the fact that Mg plays an important role in chlorophyll synthesis (Guo et al., 2016), comparison of the effect of rGO and Mg/rGO NCs at the same concentrations indicated that the positive impacts of Mg/rGO can be attributed to the presence of Mg NPs in the construction of these NCs. Some other studies have also shown the positive effect of Mg and MgO NPs on the biosynthesis of photosynthetic pigments and photosynthesis efficiency (Raliya et al., 2014; Rathore and Tarafdar, 2015). Such information may help to boost crop production or design of artificial light-harvesting systems in the future (Giraldo et al., 2014; Mingfang et al., 2013).

Phytochemical assay and metabolic profile

Metabolomics is one of the most important approaches for evaluating the plant response to different stress conditions. Among the multiple analytical techniques, GC-MS is a fully developed method for plant metabolite profiling which analyzes several chemical compounds including sugars, organic acids, amino acids, sugar alcohols, aromatic amines and fatty acids (Shulaev et al., 2008). Therefore, in the present study, the changes in the chemical compounds induced by rGO and Mg/rGO NCs were detected after 28 days of exposure in *M. longifolia* shoot cultures. The overall chemical profiles of the n-hexane extracts, the identity, and the percentage content of the components are briefly presented in Table 4 and their chemical class distribution are also reported in Table 5. According to the GC-MS results, 118 components were separated. The extract obtained from control cultures was characterized by the presence of oxygenated monoterpenes (57.95%), phenolic componds (20.42%) and substituted aromatic hydrocarbons (0.45%) which composed 78.82% of the total compounds of the extract. Thymol (26.72%), carvacrol (21.60%), bis-(2-ethylhexyl) phthalate (19.97%), and o-cymen-5-ol (9.63%) were the main compounds in the extract of the control plants. The total content of compounds was higher in the treatments of 25 (84.15%), 50 (96.15%), and 100 (92.76%) mg/L of rGO as well as 25 (97.81%), 50 (92.20%), and 100 (93.02%) mg/L of Mg/rGO NCs in comparison with the control (78.82%) (Table 5). In agreement with our results, essential oils increase was also observed in some species of Lamiaceae family under abiotic stresses including TiO_2 NPs (Ghorbanpour, 2015; Taarit et al., 2010). The highest amount of aliphatic hydrocarbons (24.53%) including heptacosane and nonacosane, fatty acids (13.55%) such as linoleic acid, tetradecanoic acid, and stearic acid, along with oxygenated diterpenes (5.65%) for instance sclareoloxide, phytol were observed in the cultures after exposure to 25 mg/L of rGO. Oxygenated monoterpenes, including L-carvone, thymol, o-Cymen-5-ol, carvacrol, and neryl propanoate, were found to be the major metabolites in approximately all treatments except for 25 mg/L of rGO. However, monoterpene hydrocarbons, including α-pinene, β-myrcene, α-thujene, α-phellandrene, β-phellandrene and sabinene, were only observed in the treatment of 25 mg/L of Mg/rGO NCs; β-pinene was observed in the treatments of 25 and 50 mg/L of Mg/rGO NCs. Besides, bis-(2-ethylhexyl) phthalate was identified in high concentrations under the NMs stress with the exception of 100 mg/L of rGO. High levels of oxygenated sesquiterpenes (for example α-bisabolol and α-cadinol) and sesquiterpene hydrocarbons (for example germacrene D, α-copaene, trans-β-farnesene, and δ-cadinene) were determined in the treatments of 25 mg/L of rGO (8.03%) and Mg/rGO NCs (15.37%), respectively. The most abundant oxygenated triterpene was friedelan-3-one constituted 30.13% of the extract of the cultures treated with 50 mg/L of rGO. GC-MS analysis of the extracts showed the abundance of oxygenated terpenoids in the treated cultures with rGO. It has been demonstrated that the difference in chemical structure and saturation of terpenoids are the key factors influencing the potential biological activity of the essential oils. oxygenated terpenoids are described to have the higher antimicrobial and antioxidant activities than the non-oxygenated ones (Kumar et al., 2011). Therefore, it seems that the elevation of these bioactive compounds might exhibit protective role against the stress caused by the NMs. Consequently, considering the medicinal importance of bioactive compounds, application of the effective concentrations of rGO and Mg/rGO NCs as an elicitor can be a suitable approach to manipulate the content and type of the secondary metabolites.

Conclusion

The current study proposed the green synthesis of rGO and Mg/rGO NCs and presented new insights on their impacts on *M. longifolia* growth and metabolism. The applied characterization techniques indicated the preparation of rGO and Mg/rGO NCs via an eco-friendly chemical reduction method. Besides, cytotoxicity results evidenced the adverse effects of rGO on the biosynthesis of photosynthetic pigments and the growth of *M. longifolia in vitro* cultures. In contrast, Mg/rGO NCs showed to be quite biocompatible compared with rGO. Both rGO and Mg/rGO NCs caused a gradual increase in total volatile compounds content at the concentrations ranging from 25 to 100 mg/L. Generally, the more oxygenated and hydrocarbon sesquiterpenes was observed in the cultures treated with 25 and 100 mg/L of rGO and 25 and 50 mg/L of Mg/rGO NCs. Accordingly, detailed studies are necessary to investigate the ability of Mg/rGO NCs as Mg nano-biofertilizer to sustain high crop yield or better-quality of medicinal plants.

Declarations

Data availability Data is available by request to the corresponding author.

Ethics approval and consent to participate

Not applicable.

Consent for publication

Not applicable.

Competing interest

The authors have no conflicts of interest to declare that are relevant to the content of this article.

Acknowledgement

The authors wish to thank the University of Tabriz for financial supports.

References

1. Alavi, M. A., Morsali, A., 2010. Syntheses and characterization of $Mg(OH)_2$ and MgO nanostructures by ultrasonic method. Ultrason Sonochem. 17, 441-446.
2. Anjum, N. A., Singh, N., Singh, M. K., Shah, Z. A., Duarte, A. C., Pereira, E., Ahmad, I., 2013. Single-bilayer graphene oxide sheet tolerance and glutathione redox system significance assessment in faba bean (*Vicia faba* L.). J. Nanoparticle Res. 15, 1770.
3. Asghari, B., Zengin, G., Bahadori, M. B., Abbas-Mohammadi, M., Dinparast, L., 2018. Amylase, glucosidase, tyrosinase, and cholinesterases inhibitory, antioxidant effects, and GC-MS analysis of

wild mint (*Mentha longifolia* var. *calliantha*) essential oil: A natural remedy. Eur. J. Integr. *Med.* 22, 44-49.

4. Asif, S. A. B., Khan, S. B., Asiri, A. M., 2017. Assessment of graphene oxide/MgAl oxide nanocomposite as a non-enzymatic sensor for electrochemical quantification of hydrogen peroxide. J Taiwan Inst Chem Eng. 74, 255-262.
5. Atarod, M., Nasrollahzadeh, M., Sajadi, S. M., 2015. Green synthesis of a Cu/reduced graphene oxide/Fe_3O_4 nanocomposite using *Euphorbia wallichii* leaf extract and its application as a recyclable and heterogeneous catalyst for the reduction of 4-nitrophenol and rhodamine B. RSC Adv. 5, 91532-91543.
6. Barazani, O., Fait, A., Cohen, Y., Diminshtein, S., Ravid, U., Putievsky, E., Lewinsohn, E., Friedman, J., 1999. Chemical variation among indigenous populations of *Foeniculum* vulgare var. *vulgare* in Israel. Planta Med. 65, 486-489.
7. Begum, P., Ikhtiari, R., Fugetsu, B., 2011. Graphene phytotoxicity in the seedling stage of cabbage, tomato, red spinach, and lettuce. Carbon. 49, 3907-3919.
8. Behzad, F., Jafarirad, S., Samadi, A., Barzegar, A., 2020. A systematic investigation on spectroscopic, conformational, and interactional properties of polypeptide/nanomaterial complex: effects of bio-based synthesized maghemite nanocomposites on human serum albumin. Soft Mater. 1-16.
9. Benzon, H. R. L., Rubenecia, M. R. U., Ultra Jr, V. U., Lee, S. C., 2015. Nano-fertilizer affects the growth, development, and chemical properties of rice. *International* IJAAR. 7, 105-117.
10. Bhargava, R., Khan, S., 2017. Effect of reduced graphene oxide (rGO) on structural, optical, and dielectric properties of $Mg(OH)_2$/rGO nanocomposites. Adv Powder Technol. 28, 2812-2819.
11. Chen, D., Feng, H., Li, J., 2012. Graphene oxide: preparation, functionalization, and electrochemical applications. Chem. Rev. 112, 6027-6053.
12. Cheng, F., Liu, Y.-F., Lu, G.-Y., Zhang, X.-K., Xie, L.-L., Yuan, C.-F., Xu, B.-B., 2016. Graphene oxide modulates root growth of *Brassica napus* L. and regulates ABA and IAA concentration. J. Plant Physiol. 193, 57-63.
13. De Silva, K., Huang, H.-H., Joshi, R., Yoshimura, M., 2017. Chemical reduction of graphene oxide using green reductants. Carbon 119, 190-199.
14. Ebadollahi, R., Jafarirad, S., Kosari-Nasab, M., Mahjouri, S., 2019. Effect of explant source, perlite nanoparticles and TiO_2/perlite nanocomposites on phytochemical composition of metabolites in callus cultures of Hypericum perforatum. Sci. Rep. 9, 1-15.
15. Fan, X., Zhang, G., Zhang, F., 2015. Multiple roles of graphene in heterogeneous catalysis. Chem. Soc. Rev. 44, 3023-3035.
16. Ghorbanpour, M., 2015. Major essential oil constituents, total phenolics and flavonoids content and antioxidant activity of *Salvia officinalis* plant in response to nano-titanium dioxide. Indian J. Plant Physiol. 20, 249-256.

17. Giraldo, J. P., Landry, M. P., Faltermeier, S. M., McNicholas, T. P., Iverson, N. M., Boghossian, A. A., Reuel, N. F., Hilmer, A. J., Sen, F., Brew, J. A., 2014. Plant nanobionics approach to augment photosynthesis and biochemical sensing. Nat. Mater. 13, 400-408.
18. Guo, W., Nazim, H., Liang, Z., Yang, D., 2016. Magnesium deficiency in plants: an urgent problem. Crop J. 4, 83-91.
19. Hazeem, L. J., Bououdina, M., Dewailly, E., Slomianny, C., Barras, A., Coffinier, Y., Szunerits, S., Boukherroub, R., 2017. Toxicity effect of graphene oxide on growth and photosynthetic pigment of the marine alga *Picochlorum* sp. during different growth stages. Environ. Sci. Pollut. Res. 24, 4144-4152.
20. Hu, X., Lu, K., Mu, L., Kang, J., Zhou, Q., 2014. Interactions between graphene oxide and plant cells: regulation of cell morphology, uptake, organelle damage, oxidative effects and metabolic disorders. Carbon 80, 665-676.
21. Huang, X., Qi, X., Boey, F., Zhang, H., 2012. Graphene-based composites. Chem. Soc. Rev. 41, 666-686.
22. Jafarirad, S., Hammami Torghabe, E., Rasta, S. H., Salehi, R., 2018. A novel non-invasive strategy for low-level laser-induced cancer therapy by using new Ag/ZnO and Nd/ZnO functionalized reduced graphene oxide nanocomposites. Artif Cells Nanomed Biotechnol. 46, 800-816.
23. Jafarirad, S., Salmasi, M., Divband, B., Sarabchi, M. (2019). Systematic study of Nd3+ on structural properties of ZnO nanocomposite for biomedical applications; in-vitro biocompatibility, bioactivity, photoluminescence and antioxidant properties. J. Rare Earths. 37, 508-514.
24. Julkapli, N. M., Bagheri, S., 2015. Graphene supported heterogeneous catalysts: an overview. Int. J. Hydrog. Energy. 40, 948-979.
25. Kanagesan, S., Hashim, M., Tamilselvan, S., Alitheen, N., Ismail, I., Bahmanrokh, G., 2013. Cytotoxic effect of nanocrystalline $MgFe_2O_4$ particles for cancer cure. J. Nanomater. 2013.
26. Kandiban, M., Vigneshwaran, P., Potheher, I. V., 2015. Synthesis And Characterization Of Mgo Nanoparticles For Photocatalytic Applications. In "National Conference On Recent Trends In Crystal Growth And Advancement". 3, 248-254.
27. Kumar, P., Mishra, S., Malik, A., Satya, S., 2011. Insecticidal properties of *Mentha* species: a review. Ind Crops Prods. 34, 802-817.
28. Lattanzio, F., Greco, E., Carretta, D., Cervellati, R., Govoni, P., Speroni, E., 2011. In vivo anti-inflammatory effect of *Rosa canina* L. extract. J. Ethnopharmacol. 137, 880-885.
29. Li, J.-L., Tang, B., Yuan, B., Sun, L., Wang, X.-G., 2013. A review of optical imaging and therapy using nanosized graphene and graphene oxide. Biomaterials. 34, 9519-9534.
30. Marslin, G., Sheeba, C. J., Franklin, G., 2017. Nanoparticles alter secondary metabolism in plants via ROS burst. Front. Plant Sci. 8, 832.
31. Mikaili, P., Mojaverrostami, S., Moloudizargari, M., Aghajanshakeri, S., 2013. Pharmacological and therapeutic effects of *Mentha Longifolia* L. and its main constituent, menthol. Anc. Sci. Life. 33, 131-138.

32. Mingfang, Q., Yufeng, L., Tianlai, L., 2013. Nano-TiO_2 improve the photosynthesis of tomato leaves under mild heat stress, biological trace element research. Biol. Trace Elem. Res. 156, 323-328.
33. Mohammadi, H., Esmailpour, M., Gheranpaye, A., 2016. Effects of TiO_2 nanoparticles and water-deficit stress on morpho-physiological characteristics of dragonhead (*Dracocephalum moldavica* L.) plants. Acta Agric. Slov. 107, 385-396.
34. Nazari, F., Jafarirad, S., Movafeghi, A., Kosari-Nasab, M., Kazemi, E. M., 2020. Toxicity of microwave-synthesized silver-reduced graphene oxide nanocomposites to the microalga Chlorella vulgaris: Comparison with the hydrothermal method synthesized counterparts. J. Environ. Sci. Health A. 55, 639-649.
35. Nazari, F., Movafeghi, A., Jafarirad, S., Kosari-Nasab, M., and Divband, B., 2018. Synthesis of reduced graphene oxide-silver nanocomposites and assessing their toxicity on the Green microalga *Chlorella vulgaris*. J. Bionanosci. 8, 997-1007.
36. Raliya, R., Tarafdar, J., Singh, S., Gautam, R., Choudhary, K., Maurino, V. G., Saharan, V., 2014. MgO nanoparticles biosynthesis and its effect on chlorophyll contents in the leaves of clusterbean (*Cyamopsis tetragonoloba* L.). Adv Sci Eng Med. 6, 538-545.
37. Rathore, I., Tarafdar, J., 2015. Perspectives of biosynthesized magnesium nanoparticles in foliar application of wheat plant. J. Bionanosci. 9, 209-214.
38. Rezaei, Z., Jafarirad, S., Kosari-Nasab, M., 2019. Modulation of secondary metabolite profiles by biologically synthesized MgO/perlite nanocomposites in Melissa officinalis plant organ cultures. J. Hazard. Mater. 380, 120878.
39. Roman, I., Stanila, A., Stanila, S., 2013. Bioactive compounds and antioxidant activity of *Rosa canina* L. biotypes from spontaneous flora of Transylvania. Chem. Cent. J. 7, 73.
40. Shulaev, V., Cortes, D., Miller, G., Mittler, R., 2008. Metabolomics for plant stress response. Physiol. Plant. 132, 199-208.
41. Subramanian, K. S., Manikandan, A., Thirunavukkarasu, M., Rahale, C. S., 2015. Nano-fertilizers for balanced crop nutrition. In "Nanotechnologies in Food and Agriculture" (R. C. Rai M., Mattoso L., Duran N., ed.), 69-80. Springer.
42. Taarit, M. B., Msaada, K., Hosni, K., Marzouk, B., 2010. Changes in fatty acid and essential oil composition of sage (*Salvia officinalis* L.) leaves under NaCl stress. Food Chem. 119, 951-956.
43. Tan, C., Huang, X., Zhang, H., 2013. Synthesis and applications of graphene-based noble metal nanostructures. Mater. Today. 16, 29-36.
44. Thakur, S., Karak, N., 2012. Green reduction of graphene oxide by aqueous phytoextracts. Carbon. 50, 5331-5339.
45. Tumbas, V. T., Canadanovic-Brunet, J. M., Cetojevic-Simin, D. D., Cetkovic, G. S., Dilas, S. M., and Gille, L., 2012. Effect of rosehip (*Rosa canina* L.) phytochemicals on stable free radicals and human cancer cells. J. Sci. Food Agric. 92, 1273-1281.

46. ullah Rather, S., 2014. Synthesis, characterization, and hydrogen uptake studies of magnesium nanoparticles by solution reduction method. Mater. Res. Bull. 60, 556-561.
47. Upadhyay, R. K., Soin, N., Bhattacharya, G., Saha, S., Barman, A., Roy, S. S., 2015. Grape extract assisted green synthesis of reduced graphene oxide for water treatment application. Mater. Lett. 160, 355-358.
48. Van den Dool, H., and Kratz, P. D., 1963. "A generalization of the retention index system including linear temperature programmed gas-liquid partition chromatography."
49. Veisi, H., Rashtiani, A., Barjasteh, V., 2016. Biosynthesis of palladium nanoparticles using *Rosa canina* fruit extract and their use as a heterogeneous and recyclable catalyst for Suzuki–Miyaura coupling reactions in water. Appl. Organomet. Chem. 30, 231-235.
50. Wang, G., Shen, X., Yao, J., Park, J., 2009. Graphene nanosheets for enhanced lithium storage in lithium ion batteries. Carbon. 47, 2049-2053.
51. Wellburn, A. R. 1994. The spectral determination of chlorophylls a and b, as well as total carotenoids, using various solvents with spectrophotometers of different resolution. J. Plant Physiol. 144, 307-313.
52. Wu, B., Zhu, L., Le, X. C., 2017. Metabolomics analysis of TiO_2 nanoparticles induced toxicological effects on rice (*Oryza sativa* L.). Environ. Pollut. 230, 302-310.
53. Wu, S., Ge, R., Lu, M., Xu, R., Zhang, Z., 2015. Graphene-based nano-materials for lithium–sulfur battery and sodium-ion battery. Nano Energy. 15, 379-405.
54. Zhao, S., Wang, Q., Zhao, Y., Rui, Q., Wang, D., 2015. Toxicity and translocation of graphene oxide in *Arabidopsis thaliana*. Environ. Toxicol. Pharmacol. 39, 145-156.
55. Zhu, J., Wang, J., Hou, J., Zhang, Y., Liu, J., Van der Bruggen, B., 2017. Graphene-based antimicrobial polymeric membranes: a review. J. Mater. Chem. A. 5, 6776-6793.

Tables

Due to technical limitations, tables are only available as a download in the Supplemental Files section.

Figures

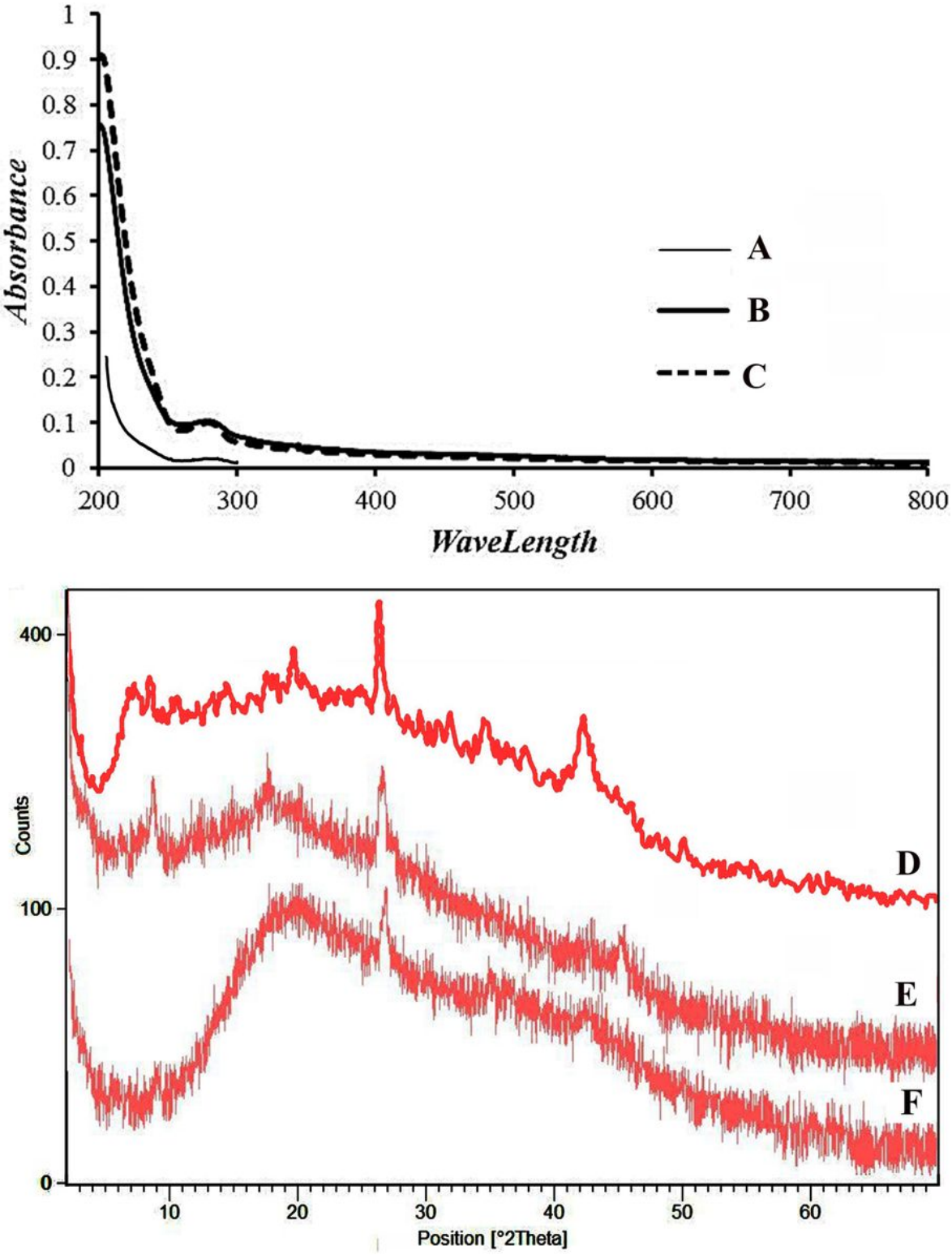

Figure 1

UV-Vis spectrums of rGO (A) and Mg/rGO NCs prepared by H (B) and M (C) methods; XRD patterns of rGO (D) and Mg/rGO NCs prepared by H (E) and M (F) methods.

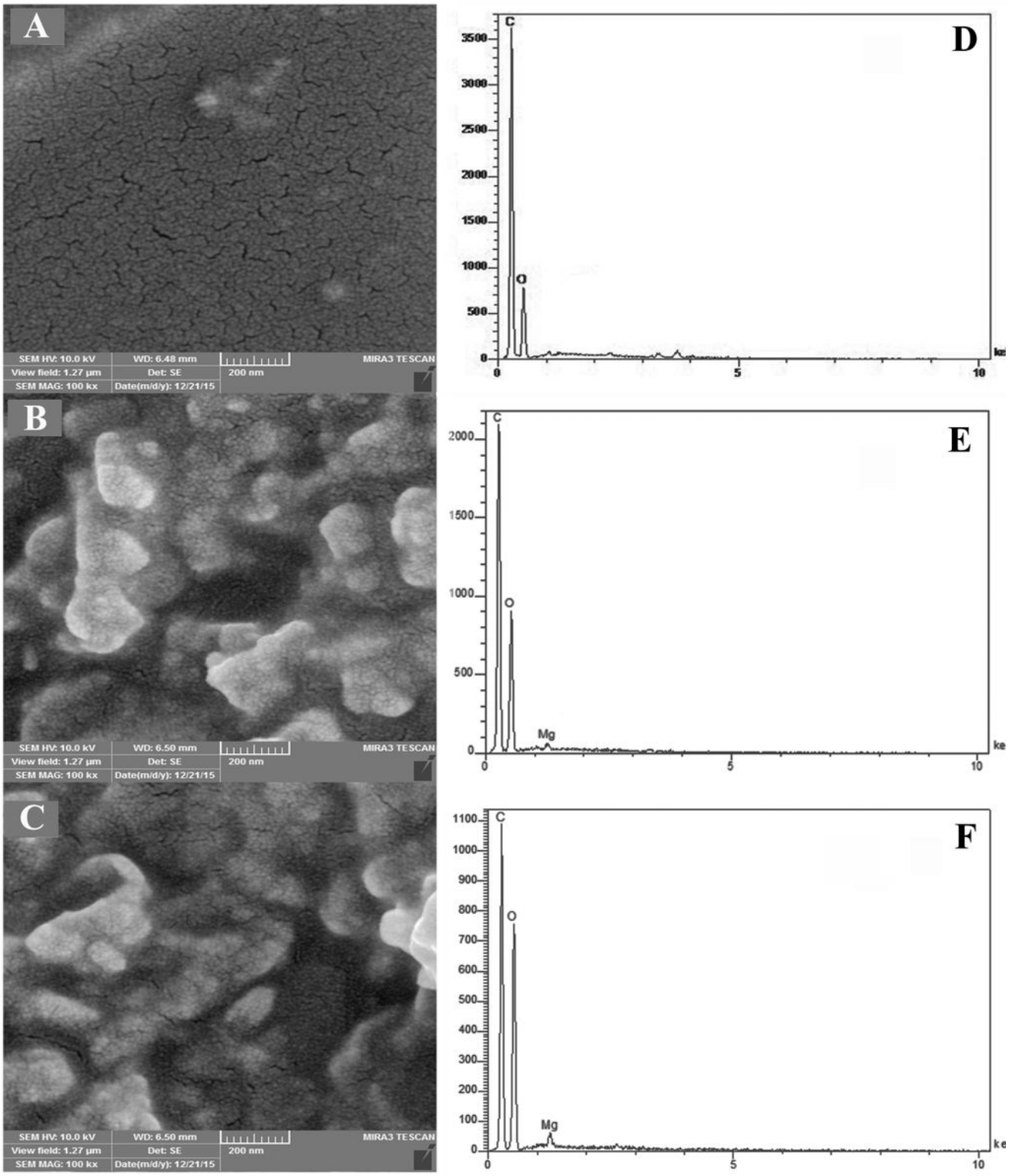

Figure 2

FESEM images of rGO (A) and Mg/rGO NCs prepared by H (B) and M (C) method; EDX spectrum of rGO (D) and Mg/rGO NCs prepared by H (E) and M (F) methods.

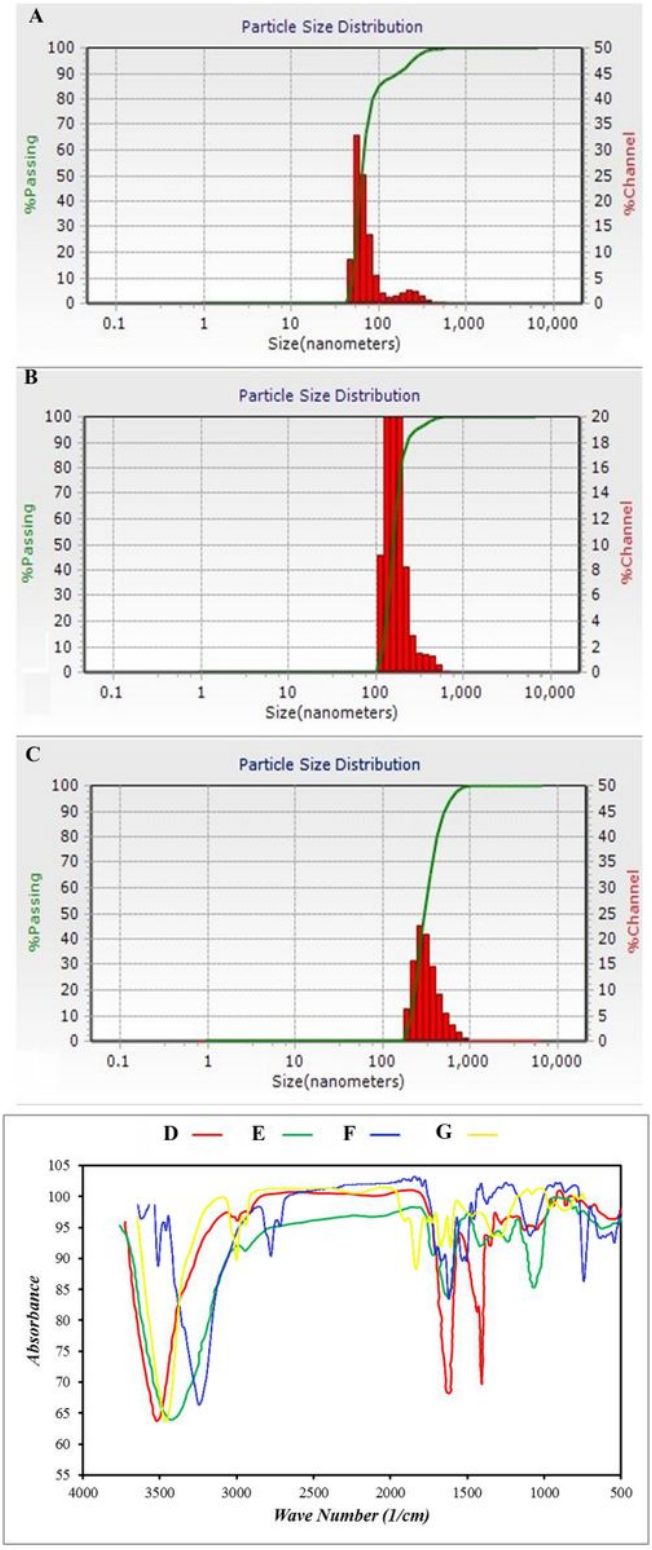

Figure 3

DLS patterns of rGO (A) and Mg/rGO NCs prepared by H (B) and M (C) methods; FT-IR spectra of R. canina fruit extract (D), rGO (E), and Mg/rGO NCs prepared by H (F) and M (G) methods.

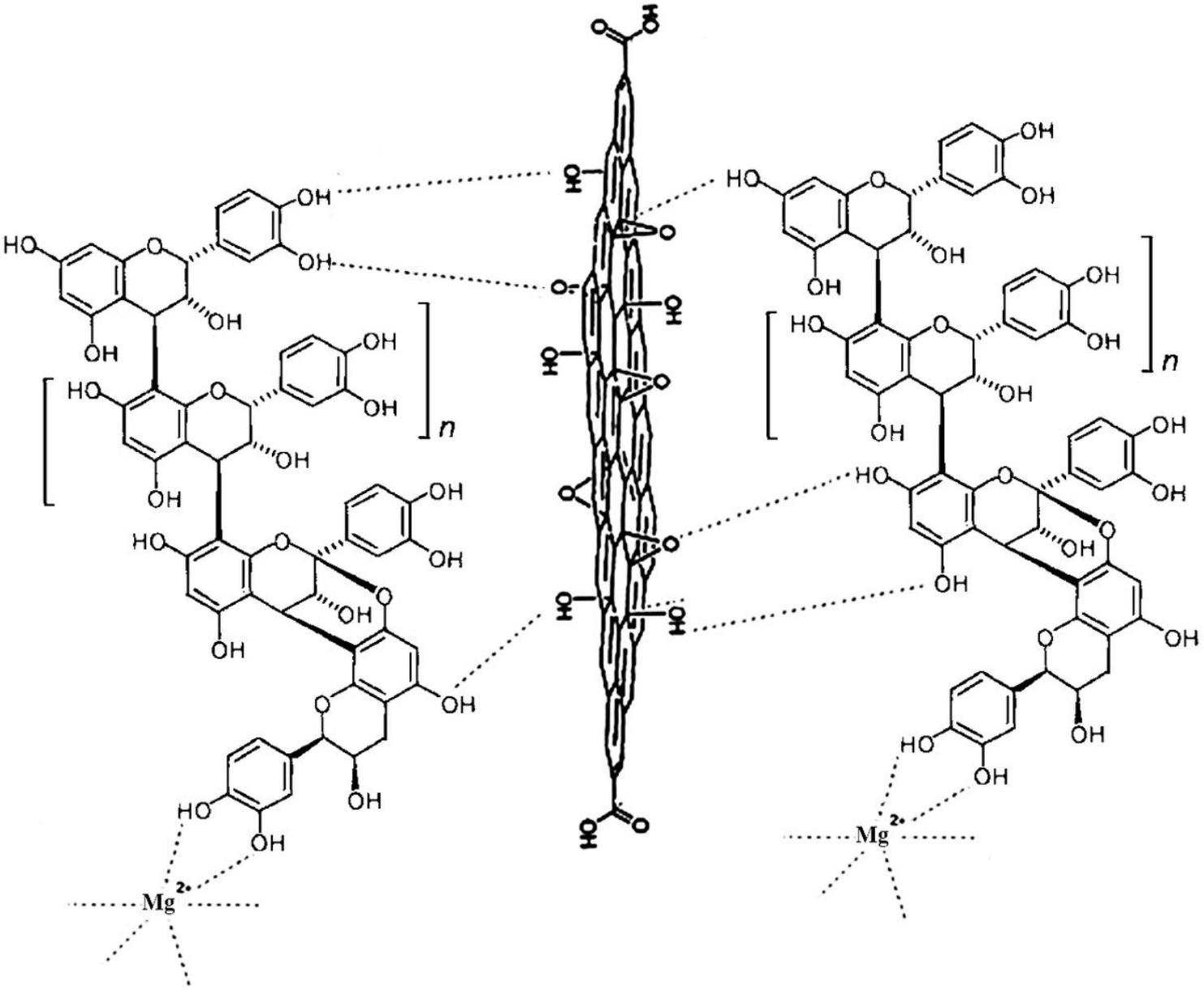

Figure 4

The proposed mechanism for stabilizing stage of the Mg/rGO NCs using A-type proanthocyanidin as a polyphenol in the aqueous extract of R. canina fruit extract.

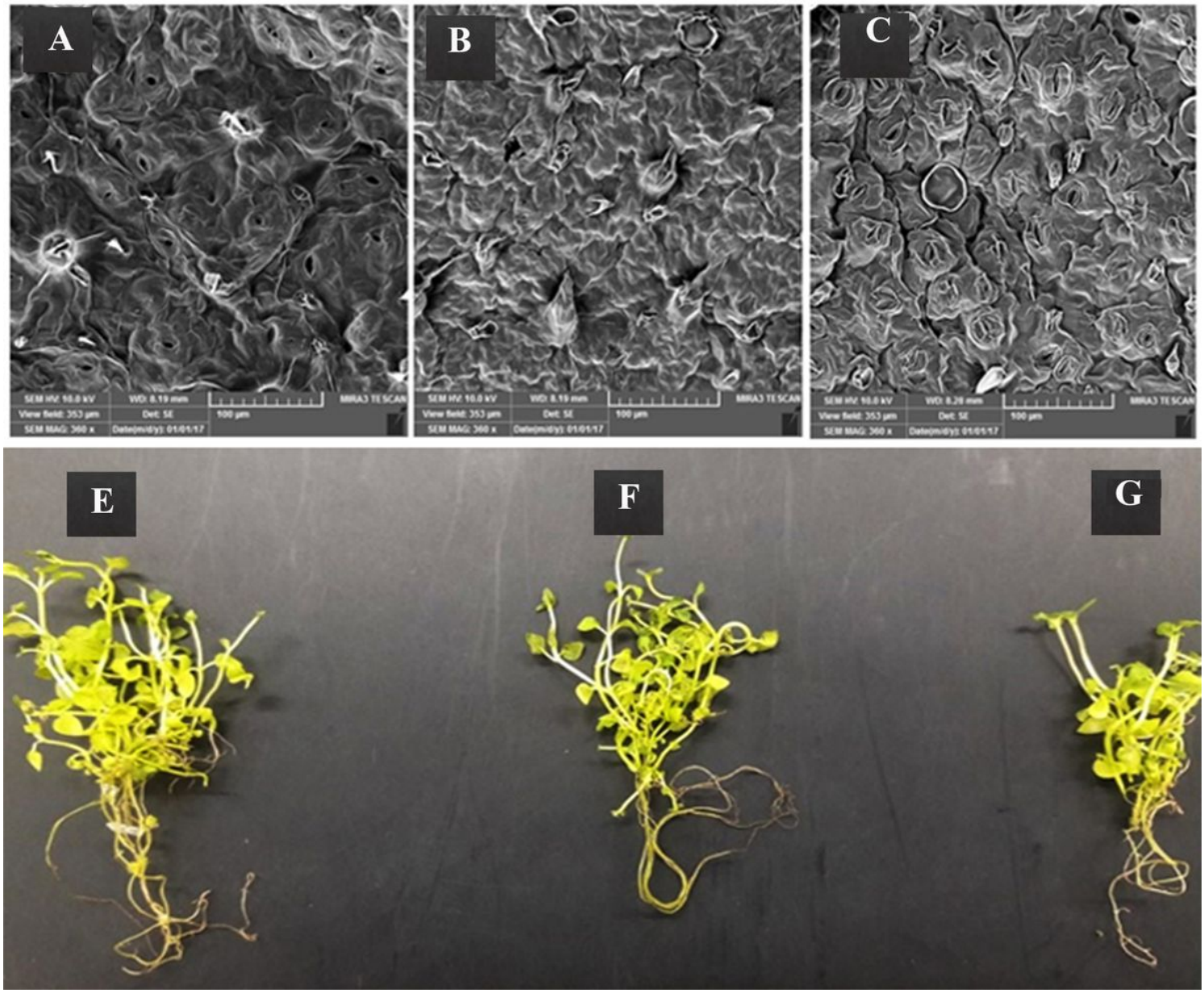

Figure 5

SEM observations of the leaf surface of the control and treated plants with 150 mg/L of rGO and Mg/rGO NCs. Control leaf (A), rGO treated leaf (B) and Mg/rGO NCs treated leaf (C); Morphology of the untreated M. longifolia plants (D) and the treated plants with 150 mg/L of Mg/rGO NCs (E) and rGO (F).

Supplementary Files

This is a list of supplementary files associated with this preprint. Click to download.

- graphicalabstractaminpoor.tif
- Tables.docx